J Water Environ Nanotechnol 2026, 11(1): 17-29
10.22090/jwent.2026.01.02

RESEARCH PAPER

Enhancing Ceramic Membrane Support Properties with Biowaste: Effects of Particle Size Distribution and Sintering Temperature

Mehdi Simiari[1]*, *Hassan Tavakoli*[2]

[1]Department of Physics, Faculty of Basic Science, Imam Ali University, Tehran, Iran
[2]Chemistry Group, Faculty of Basic Science, Imam Ali University, Tehran, Iran

* Corresponding Author.
Department of Physics, Faculty of Basic Science, Imam Ali University, Tehran, Iran
Email: mahdi.simiari@gmail.com

Article History:
Received: 2025-07-25
Revised: 2025-10-11
Accepted: 2025-12-05

How to cite this article
Simiari M, Tavakoli H. Enhancing Ceramic Membrane Support Properties with Biowaste: Effects of Particle Size Distribution and Sintering Temperature. J Water Environ Nanotechnol 2026, 11(1): 17-29, DOI: 10.22090/jwent.2026.01.02

HIGHLIGHTS

- Incorporated 5 wt% eggshell powder as a pore-former into α-Al_2O_3 ceramic membranes.
- Demonstrated that sintering temperatures (1250 °C, 1350 °C, 1450 °C) influence porosity and mechanical strength.
- Found that grossite ($CaAl_4O_7$) formation enhances bending strength.
- Observed that larger eggshell particles (10 µm) increase porosity, while smaller particles (2 µm) improve mechanical properties.
- Highlighted the potential of eggshell powder as a sustainable biowaste material for ceramic membrane fabrication.

ABSTRACT

Eggshell waste, a common by-product of the food industry, creates both environmental and disposal concerns. In this study, we examine how eggshell powder can serve as an environmentally friendly pore-forming agent in the gel-casting production of α-Al_2O_3 ceramic membranes, to improve membrane performance while giving new value to this biowaste. Eggshell powders with particle sizes of 2 µm, 4 µm, and 10 µm (5 wt. %) were incorporated into α-Al_2O_3 (95 wt. %) and compared with pure α-Al_2O_3 membranes. Membranes were sintered at 1250 °C, 1350 °C, and 1450 °C, and characterized for porosity, shrinkage, mechanical strength, and water flux. The addition of eggshell powder increased porosity from 43% (pure α-Al_2O_3) to 57.23% (10 µm, 1450 °C) and reduced linear shrinkage by up to 50%. Mechanical strength improved with smaller particle sizes, reaching 4.94 MPa for 2 µm particles at 1450 °C, compared with 3.43 MPa for pure α-Al_2O_3. The membranes containing 10 µm eggshell particles showed a marked increase in water flux, reaching 1860 LMH at 1450 °C compared with 1250 LMH for the pure α-Al_2O_3 sample. This result shows that adding eggshell powder can improve membrane performance while offering a practical, sustainable way to reuse biowaste in ceramic production, transforming a waste problem into a practical technological solution.

KEYWORDS: Eggshell, Alumina, Gel Casting, Inorganic membrane.

©2026 The Author(s). Published by the Iranian Environmental Mutagen Society. This work is licensed under the Creative Commons Attribution 4.0 International License (CC BY 4.0). To view a copy of this license, visit http://creativecommons.org/licenses/by/4.0/.

1. INTRODUCTION

Ceramic membranes are well known for many benefits, such as long-lasting endurance, superior structural integrity, resistance to corrosive agents, and heat tolerance. Ceramic membrane is usually made of oxides of aluminum, zirconium, and titanium [1]. Although ceramic compounds critically influence the performance of ceramic membranes, the choice of binder and pore former is also essential for determining the membrane's properties [2]. It is essential to understand that an increase in porosity typically leads to a decrease in mechanical strength [3].

Pore formers are critical in adjusting the structural characteristics of ceramic membranes. By incorporating pore formers, durable pores can be formed, along with additional options to strengthen chemical robustness [4]. Optimal functionality can be achieved by balancing microstructure (i.e., porosity and pore size) and mechanical properties [5]. Waste biomaterials for ceramic membrane pore formers present a sustainable use of material, as the principles of industrial ecology highlight waste material recycling and reuse in a closed-loop system to minimize ecological footprint. Valorization of agricultural residues as alternative renewable feedstock decreases the primary resource dependence and provides multiple green economy benefits [6-8].

Eggshells (ES), which are discarded as waste, have a complex fibrous structure composed of glycoproteins and collagen. Also, structured bio-macromolecules have various groups such as hydroxyl, thiol, carboxyl, amino, amide, etc. It has always been proven in previous studies that eggshells have been introduced as one of the environmental problems in countries where the egg production industry is well developed. Approximately 8.5 million tons of eggshell waste are produced annually. ES contains about 95% calcium carbonate in the form of calcite and 5% organic matter (Al_2O_3, SiO_2, S, Cl, P, and Cr_2O_3, MgO) such as type X collagen, sulfated polysaccharides, and other proteins [9]. This transformation of abundant by-products into useful resources addresses the problems of waste management and makes a contribution toward material sustainability [10]. The addition of eggshell powder in ceramic composites will improve mechanical properties, make microstructural changes, and favor chemical bonding inside the ceramic matrix. Based on the results obtained, ES has a relatively lower density than inorganic calcium carbonate. Also, the structure of the eggshell consists of a protein covered with mineral crystals, which is made of a calcium compound such as calcium carbonate [11].

In the development of ceramic materials, several researchers have been studying the use of waste eggshell powder. For example, when limestone in the production of wall tiles was replaced by eggshell powder, there was an increase in the flexural strength, while there was a reduction in the consumption of natural raw materials without affecting other properties [12]. In another study, Fe-B_4C composites with the addition of eggshell powder in various proportions were sintered at 1400 °C. The porosity decreased, and hardness increased as the coarser grain structures increased within the eggshell content [13]. It was also observed that the addition of eggshell as a reinforcement agent with a porogen in ceramic clay resulted in enhanced porosity and structural strength of the specimens. Clay / Coconut shell / Eggshell sintered at 800, 900, and 1000 °C showed an optimum flux of 14,013 LMH and 90% rejection during application at the membrane [14].

In this study, we explored how adding eggshell powder of different particle sizes to α-Al_2O3 ceramic membranes—made using gel casting—affects their structure and properties. Specifically, we looked at how particle sizes of 2 μm, 4 μm, and 10 μm influence characteristics like porosity, shrinkage, and mechanical strength. It also explored the impact of sintering temperature (1250 °C, 1350 °C, and 1450 °C) on the microstructure and performance of both pure α-Al_2O_3 and eggshell-modified membranes, as well as evaluated water flux under different particle sizes and sintering conditions. In addition, we explored the potential of eggshell powder as a sustainable pore-forming additive, aiming not only to improve membrane performance but also to give new value to an abundant biowaste. This work sheds light on practical ways to enhance ceramic membranes by incorporating eco-friendly materials, supporting progress in material science while also promoting responsible and sustainable use of resources.

2. MATERIALS AND METHODS

2.1 Raw materials

The starting materials for this work include α-Al_2O_3 (Rayra Sanat Afrand Co., Esfahan, Iran) and eggshell powder. Alpha-Al_2O_3 served as the base ceramic material, while eggshell powder was used as the additive and was milled to average particle sizes of 2, 4, and 10 μm. Raw eggshells were collected, cleaned to remove any organic residues, and dried at 105 °C for 24 h. The dried shells were then ground using a planetary ball mill. Milling times were set at 30, 60, and 90 min to produce average particle sizes of 10 μm, 4 μm, and 2 μm, respectively. In addition to these powders, acrylamide (AM, Merck Co., Germany) and N,N′-methylenebisacrylamide (MBAM, Merck Co., Germany) were used as monomer and crosslinker, respectively; ammonium persulfate (APS, Merck Co., Germany) served as the initiator; N,N,N′,N′-tetramethylethylenediamine (TEMED, Merck Co., Germany) was used as the catalyst; 4,5-dihydroxy-1,3-benzenedisulfonic acid disodium salt (Tiron, Merck Co., Germany) was added as a stabilizer; and distilled water was used as the solvent. The gel casting technique was applied to fabricate the composite membranes.

2.2 Membrane slurry preparation and casting

A 25 vol. % solids slurry was prepared as follows. The total dry powder weight was first calculated based on the target slurry volume. The dry mass mixture contained 5 wt. % eggshell powder and 95 wt. % α-Al_2O_3. The combined polymer content—AM monomer and MBAM crosslinker—was set to 7 wt. % of the dry powder mass, maintaining a monomer-to-crosslinker ratio of 10:1 by mass. APS was added at 1 wt. % of the dry powder mass as the initiator, and Tiron was incorporated at 0.1 wt. % of the dry powder mass as a stabilizer. Distilled water was added to adjust the slurry to the desired volume. Immediately before casting, TEMED was introduced at a dosage of 0.2 cc per 5 cc of slurry, based on the slurry volume placed into each mold. The mixture was then stirred thoroughly to ensure homogeneity before being cast into the molds. Then, the mixture was cast into tubular molds with a thickness of 2 mm, a length of 80 mm, and an internal diameter of 17 mm. The cast membranes were dried at room temperature until solid, and then transferred to an oven at 40 °C for 24 h before sintering.

2.3 Sintering

The sintering process was performed by heating in stages: first, heating from 25 °C to 600 °C at a 2 °C/min rate and holding for 2.5 hours; then heating from 600 °C to 1250 °C, 1350 °C, or 1450 °C at 3 °C/min and holding at the final temperature for 2 hours, then cooling naturally to ambient temperature. Experimental conditions for preparing ceramic membranes using different compositions of α-Al_2O_3 particles and eggshell powder, along with different sintering temperatures, are summarized in Table 1. Samples 1 through 3 are the control samples, containing 100% of α-Al_2O_3 without adding eggshell powder. Other samples are made from a mixture of 95% α-Al_2O_3 and 5% eggshell powder, which was used as a pore former. Sample ID gives information about each sample. For instance, "30" refers to the time in minutes that eggshell powder, used as the pore former, was ball-milled. The numbers 1, 2, and 3 refer to sintering temperatures-1250°C, 1350°C, and 1450°C, respectively. Thus, a sample labeled '30-2' would represent eggshell powder ball-milled for 30 minutes and sintered at 1350 °C.

2.4 characterization

A variety of test techniques were employed for the characterization of the composite membranes. The porosity was determined using the Archimedes technique that relies on water absorption of the material, and whose prescription has been provided by the ASTM C373-88 standard [15]. Archimedes is calculable by Eq. (1).

$$AP(\%) = \frac{w_{wet} - w_{dry}}{w_{wet} - w_{imm}} \times 100 \quad (1)$$

The weight of the ceramic sample, now referred to as W_{wet}, after immersion in distilled water for 24 hours. W_{dry} refers to the weight after it has dried in a hot air oven at 110°C for two hours, and w_{imm} represents the weight of the completely submerged ceramic.

The morphological features and structural details of membranes and powders were thoroughly elucidated through Scanning Electron Microscopy (SEM) utilizing a MIRA3-TESCAN system (TESCAN Co., Czech Republic). X-ray diffraction analysis performed, Crystallographic characterization, employing an INEL EQUINOX 3000

Table 1. Experimental conditions for α-Al_2O_3 and eggshell composition tests.

Sample ID	α-Al_2O_3 (%)	Egg Shell (%)	Sintering Temperature (°C)
1	100	0	1250
2	100	0	1350
3	100	0	1450
30-0	95	5	1250
30-1	95	5	1350
30-2	95	5	1450
60-0	95	5	1250
60-1	95	5	1350
60-2	95	5	1450
90-0	95	5	1250
90-1	95	5	1350
90-2	95	5	1450

10.22090/jwent.2026.01.02

diffractometer operating at 40 kV with Cu Kα radiation (λ = 1.5406 Å). The bending strength was quantified using a MOR-100 three-point flexural strength tester (Sanaat Saram Co., Iran). The compressive strength can be evaluated by Eq. (2) [16].

$$\sigma_f = \frac{8FLD_o}{\pi\left(D_o^4 - D_i^4\right)} \quad (2)$$

F (N) is the force of the flexural strength tester. L (m) is just the length of the membrane. Di and Do refer to the membrane's inner and outer diameters, also in meters. Finally, σ (Pa) is used to represent the flexural strength of the ceramic membrane. The inner diameter, outer diameter, and length of the ceramic membranes were measured using an Insize digital caliper, model 1108-150. X-ray fluorescence (XRF) analysis was carried out using a Philips PW1480 instrument (Philips, Netherlands), and it was employed for elemental analysis of the samples.

The performance of the ceramic membranes was checked using a cross-flow filtration system set at 1 bar.

We used Equation (3) to calculate the water flux, Jw.

$$J_w = \frac{V}{A \times t} \quad (3)$$

The permeate flux, Jw (LMH). V (L), the volume of liquid collected, A (m_2), the membrane's surface area, and t (h), the time taken to collect the liquid.

3. RESULTS AND DISCUSSION

3.1. Powder Analysis

Fig. 2A represents the SEM microstructural analysis made at a magnification of 3000x, and it indicates that the alumina particles appear with an irregular and aggregated shape, which means there is a big variation between the sizes of the particles. The powder appears to have a granular structure, where most of the particles appear between micron sizes. Apart from SEM imaging, particle size distribution was carried out, as shown

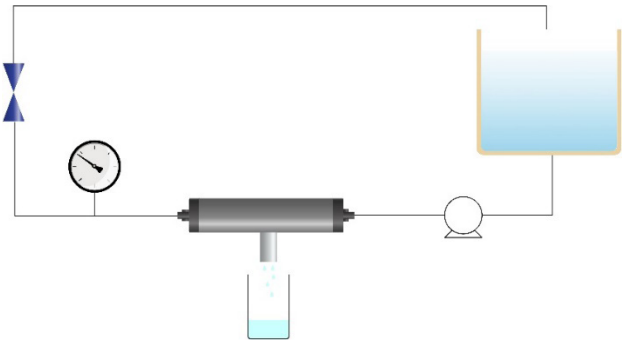

Fig. 1. Experimental setup for permeability test

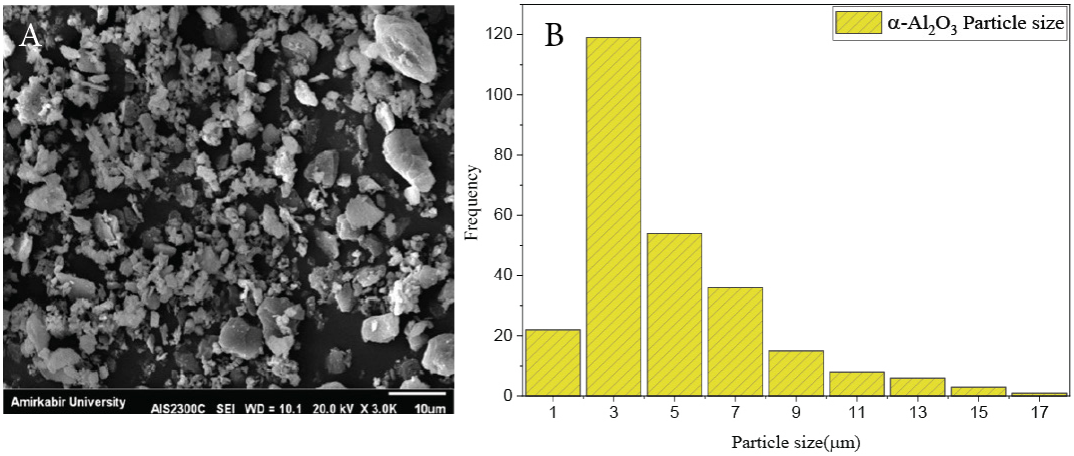

Fig. 2. (A): SEM of the morphology of alumina powder particles at 3000x and **(B)**: Particle size distribution of the α-Al_2O_3 powder.

in Fig. 2B. A frequency histogram indicated that most of the particles are within the 1 to 7 μm size range, with the peak frequency occurring at about 3 μm. It was also less frequently noticed that there is a smaller fraction of larger particles up to 17 μm. Particle size distribution characterizes the improvement in the sintering process since it influences the packing of particles, hence the quality of the sintered ceramic material [17].

The X-ray diffraction (XRD) pattern of α-Al_2O_3, shown in Fig. 3A, matches reference code 96-100-0060. This code corresponds to Aluminum oxide (Al_2O_3) with a hexagonal crystal system. The significant diffraction peaks appear at specific 2θ angles, including 25.35°, 34.82°, 37.42°, 42.95°, 52.04°, 56.97°, 60.71°, 66.06°, 67.50°, and 76.48°, each corresponding to different crystal planes (012), (104), (110), (113), (024), (116), (018), (214), (300), and (208). These sharp peaks indicate the material's high crystallinity and purity [18]. An XRF test was conducted on α-Alumina powder to determine the composition using an X-ray Fluorescence Spectrophotometer, providing a detailed elemental analysis in Table 2. As can be seen, alpha alumina with a weight percentage of 97.029% is the main composition of the sample, indicating the high purity of the alpha alumina powder used. Other components present include minor impurities such as SiO_2, Fe_2O_3, CaO, MgO, Na_2O, K_2O, TiO_2, and MnO, each of which was found in very small amounts.

Fig. 4 comprehensively shows how ball milling duration influences eggshell powder morphology and particle size

Table 2. XRF Analysis of chemical composition of Alpha Alumina Powder

Chemical Constituents	Weight Percent (%)
SiO_2	1.583
Al_2O_3	97.029
Fe_2O_3	0.318
CaO	0.174
MgO	N
Na_2O	0.7
K_2O	0.07
TiO_2	0.034
MnO	0.01
P_2O_5	N

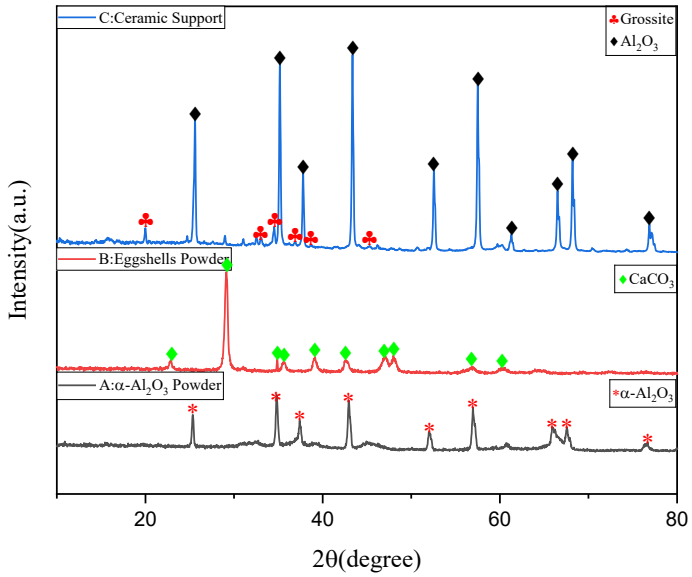

Fig. 3. X-ray diffraction (XRD) pattern of the **(A)**:α-Alumina powder, **(B)**: Egg Shell Powder, and **(C)**: ceramic membrane support with composition 95% α-Alumina and 5% Eggshell Powder

J Water Environ Nanotechnol, 2026, 11(1): 17-29
10.22090/jwent.2026.01.02

distribution. A combined examination of the SEM images and the particle size distribution histograms in Fig. 4 reveals a clear relationship between the milling time and the size of the particles.

SEM images in Fig. 4 depict that, with increasing milling time starting from 30 up to 90 min, the particles became much smaller and uniform, not only in size but also in shape. After 30 min of milling, as shown in Fig. 4a, there are relatively larger-sized particles with irregular shapes, which shows that it has just begun to break down the larger particles. After 60 minutes, Fig. 4b corresponds to finer and more delicate particles due to the longer time of milling with a mechanical effect. In Fig. 4c, after 90 minutes, a finer and well-distributed powder indicates the constant small size of the particles, which gives an idea that long milling time is effective in reducing the size of the powder.

This morphological change of the particles is reflected in the particle size distribution data represented in Fig. 4. In histogram 4a, after 30 min milling, the sizes of the particles are distributed over the broad range between 5 μm and 25 μm, with a mode at ~10 μm. After 60 minutes, the distribution in histogram 4b is significantly narrower, and most of the particles fall within the size limits from 2 μm up to 12 μm. Also, the most frequent size was reduced to about 4 μm. Finally, after 90-minute milling, in histogram 4c, one could notice that most of the particles fell into a size range of 1-7 μm with the approximate most frequent size about 2 μm.

The X-ray diffraction (XRD) pattern of the eggshell powder, shown in Fig. 3B, confirms the crystalline structure of calcium

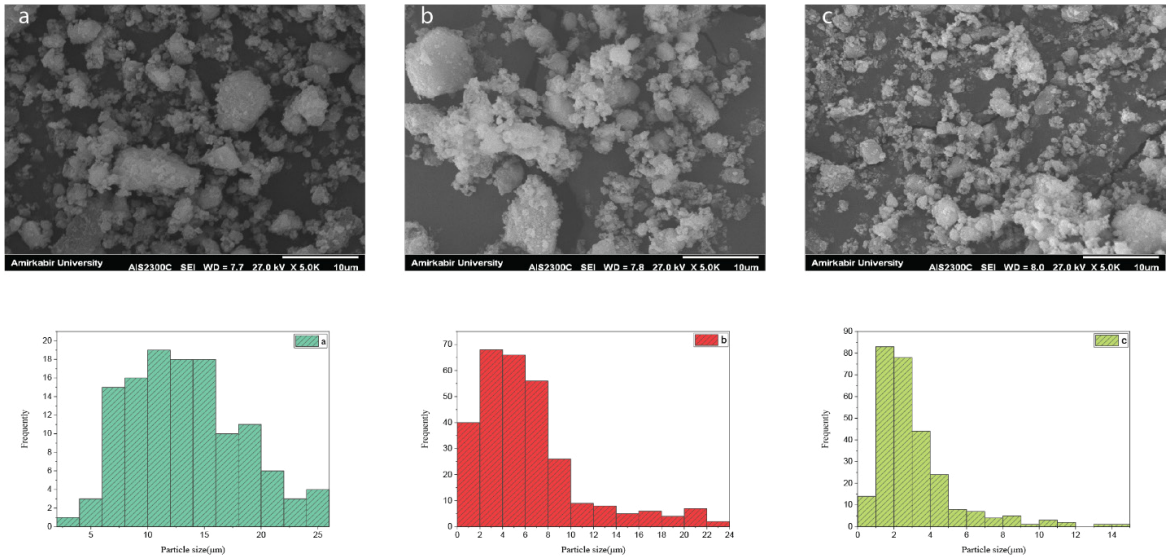

Fig. 4. SEM images of the eggshell powder ball-milled for **(a)** 30 minutes, **(b)** 60 minutes, and **(c)** 90 minutes and correspond Particle size distribution.

Table 3. XRF Analysis of the chemical composition of Egg shell Powder

Chemical constituents	Weight Percent (%)
CaO	97.4
SiO_2	0.3
Al_2O_3	0.2
K_2O	0.08
MgO	1.89
K_2O	0.07
TiO_2	0.012
MnO	0.015

carbonate ($CaCO_3$) in its calcite phase, which matches the reference code 96-702-2028. Key diffraction peaks are observed at 2θ angles of 22.83°, 29.12°, 35.62°, 39.08°, 42.67°, 47.05°, 48.04°, 56.89°, and 60.39°, corresponding to the (012), (104), (110), (113), (202), (018), (116), (211), and (122) planes, respectively [19]. Table 3 shows the chemical composition of eggshell powder determined by X-ray fluorescence (XRF) analysis. According to the data in the Table, the dominant composition in the sample is CaO with a weight percentage of 97.4%, indicating a high calcium richness of this powder. Other compositions include small amounts of oxides of silicon, aluminum, magnesium, potassium, titanium, and manganese, which were identified as impurities or minor components in the sample.

3.2. Analysis of α-Al_2O_3 Ceramic Support

Fig. 5 displays the SEM images of pure α-Al_2O_3 ceramic supports sintered at different temperatures, clearly illustrating the microstructural development as a function of sintering temperature. For the lowest sintering temperature of 1250 °C, the material has a more porous structure where the particle boundaries are clearly distinguished. Until this temperature, the particles did not fully fuse. This observation shows the material has not suffered significant densification, and its microstructure is still relatively loose and open. Increasing the sintering temperature to 1350 °C, with which the connection between α-Al_2O_3 particles forms gradually, and thus, the gaps have form a tight pore structure [20]. Increasing sintering temperature finally shows its influence; the structure appears more compact and shows evidence of grain growth at 1450 °C. The particles have sintered together more effectively, leading to a denser structure typical of higher sintering temperatures [21]. This trend shows itself in shrinkage and porosity. Linear shrinkage, diametral shrinkage, and porosity are summarized in Table 4. It is obvious that shrinkage followed a straightforward correlation with sintering temperature; as sintering temperature increased, both linear and diametral shrinkage increased. At 1250°C, linear Shrinkage and diametral Shrinkage are 5%

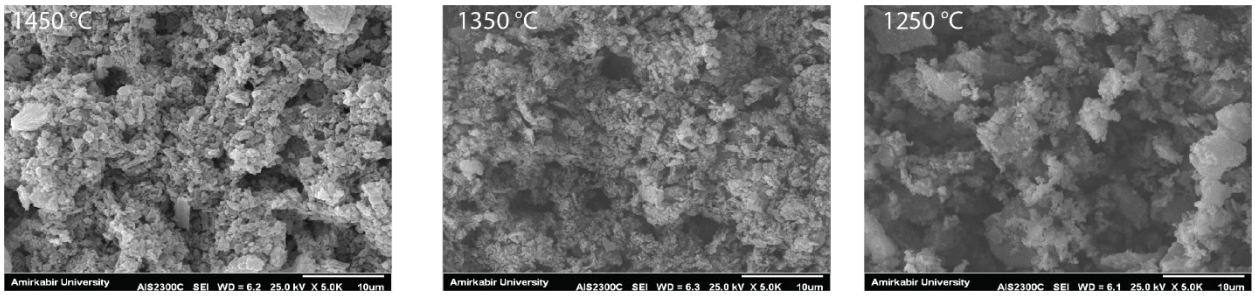

Fig. 5. SEM of pure α-Al_2O_3 ceramic support sintered at different temperatures.

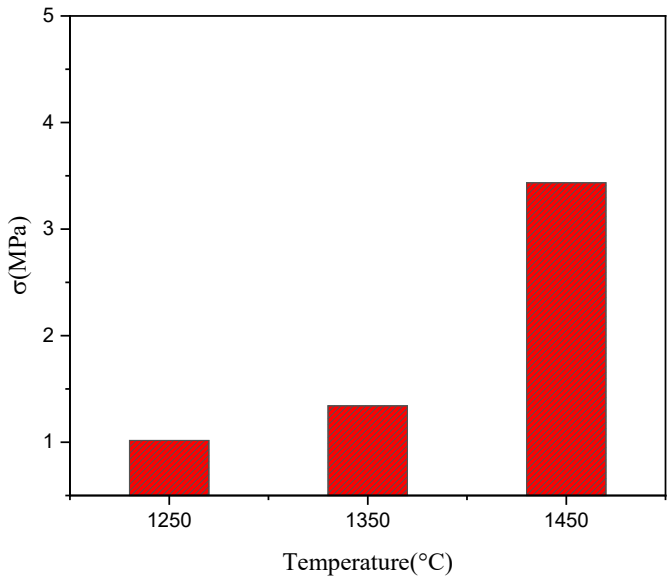

Fig. 6. Bending strength of α-Al_2O_3 as a function of sintering temperature.

J Water Environ Nanotechnol, 2026, 11(1): 17-29
10.22090/jwent.2026.01.02

Table 4. Shrinkage and porosity of pure α-Al_2O_3 ceramic support sintered at different temperatures.

Membrane	Linear Shrinkage (%) ±SD	Diametral Shrinkage (%) ±SD	Porosity (%) ±SD
1	5.00 ± 0.15	6.20 ± 0.18	48.00 ± 1.2
2	6.00 ± 0.20	7.50 ± 0.22	51.00 ± 1.0
3	10.00 ± 0.30	13.24 ± 0.35	43.00 ± 1.5

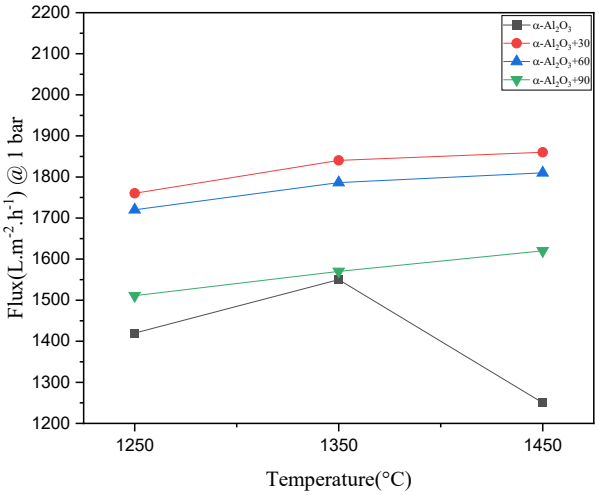

Fig. 7. Flux of ceramic membrane at 1 bar with and without the addition of eggshell as pore former.

and 6.2 %, respectively. However, the sintering temperature increased to 1350 °C, and a minor change can be seen in shrinkage. It increased by only 1%. A considerable change can be seen at increasing temperature to 1450°C. It increased to 10% for linear shrinkage and 13.24% for diametral shrinkage. However, porosity shows an increase from 1250 °C to 1350 °C. It decreased from 1350 °C to 1450 °C. This behavior is attributed to differences in sintering stages. Increasing the sintering temperature from 1250 °C to 1350 °C can be considered the initial sintering stage. In higher temperatures, grain growth and porosity decrease from 51% at 1350 °C to 43% at 1450 °C. The more extensive extent of diameter shrinkage could also be due to variations in the packing density and the influence of surface area in the radial versus axial directions during sintering [22].

The sudden decline in porosity shows that porosity has some influence on the bending strength. Fig. 6 describes the variation of sintering temperature against flexural strength. A strong correlation between sintering temperature and flexural strength could be gained. Bending strength rapidly increases with the increase of sintering temperature due to excellent densification, grain boundary diffusion, and reduced microstructural defects. The improvement is less effective from 1250 °C to 1350 °C since the material reaches a transition where grain growth tends to stabilize. Still, at 1450 °C, , the bending strength is increased as much as 2.5 times compared with that at 1350 °C. Such a high rise in sintering temperature is due to the advanced mechanism of sintering, with the increase in atomic diffusion and complete coalescence of the grains forming a more homogeneous and mechanically more robust microstructure, enhancing mechanical properties [23].

Finally, Fig. 7 shows the flux of the α-Al_2O_3 ceramic membrane at various sintering temperatures and features various stages in the microstructural changes from 1250 °C, 1350 °C, and 1450 °C. Within this 1250-1350 °C temperature range, the fluxes increase slightly from approximately 1420 LMH to approximately 1550 LMH. At this stage, particle rearrangement is dominant, favoring an increase in flux because of improved pore connectivity and structure [24]. However, complete densification still needs to occur; hence, the changes in porosity and flux are moderate. The greatest change in structure occurs between 1350 °C and 1450 °C; flux drops considerably to around 1250 LMH. This is the stage of densification where much stronger atomic diffusion occurs with grain boundary migration and elimination of pores. At this temperature, the material compacts and becomes denser, and porosity and flux decrease substantially. During this period, the routes for fluid transport become fewer due to rapid pore closure; hence, a rapid decline in flux occurs. In other words, while the particle rearrangement mechanism is dominant from 1250 °C up to 1350 °C, the densification mechanisms starting

to take place beyond 1350 °C remain associated with more pronounced porosity and flux reductions [25].

3.3. Effect of Eggshell on α-Al_2O_3 Ceramic membrane support

Adding eggshell can change the overall properties of the ceramic membrane. Fig. 8 illustrates SEM images of the ceramic membrane sintered at 1450°C, composed of 95% alpha alumina and 5% eggshell, offering insights into the microstructural changes that occur with different powder sizes of the eggshell component. These images can be compared with the previous pure α-Al_2O_3 ceramic membrane (Fig. 5) sintered under the same conditions. The pure alpha alumina membrane appears more uniform and densely packed. In contrast, the membranes containing alpha alumina and eggshell (90-2, 60-2, 30-2) exhibit distinct structural differences based on the eggshell powder size. The membrane with 2 μm eggshell particles (Fig.8A) shows smaller, more compact grains. The eggshell likely acts as a grain growth inhibitor. As the eggshell particle size increases to 4 μm (Fig. 8B), the membrane exhibits larger grains and a looser structure, with more visible pores. Finally, the most pronounced changes are on the membrane with the most considerable eggshell particle size, 10 μm. Indeed, the grain structure is much more significant, with much larger voids between the grains, indicating high porosity. With an increase in the size of the eggshell particles, the grains become much less cohesive and result in a more open, porous structure.

A change in microstructure shows its influence on other parameters. Fig. 9 illustrates the bending strength of membranes across different sintering temperatures (1250°C, 1350°C, and 1450°C). The presence of 5% eggshell powder with varying particle sizes (10 μm, 4 μm, and 2 μm) shows noticeable differences compared to pure alpha alumina, as previously shown in Fig. 6. A key observation here is that the addition of eggshell powder, particularly at smaller particle sizes, not only enhances the mechanical strength of the ceramic membrane but also modulates the shrinkage behavior,

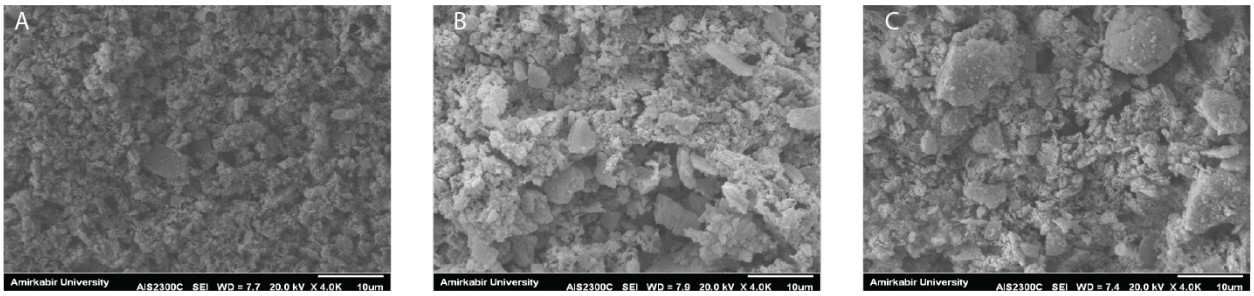

Fig. 8. SEM of Ceramic Membrane with the addition of different sizes of Egg Shell **(A)**:90-2, **(B)**:60-2, **(C)**:30-2, and sintered at 1450 °C.

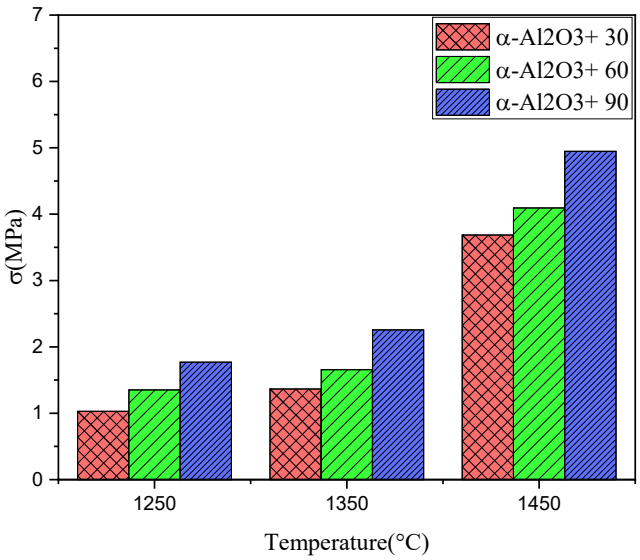

Fig. 9. Bending strength of ceramic membrane with the addition of different sizes of eggshell powder

J Water Environ Nanotechnol, 2026, 11(1): 17-29
10.22090/jwent.2026.01.02

especially by blocking densification as presented in Table 5. Regarding bending strength (Fig. 9), the composite's strength increases significantly at higher temperatures with decreasing eggshell particle size in all samples. For example, at 1450 °C, the smallest particle size (2 μm, represented as 90) reaches a bending strength of approximately 5 MPa, which is higher compared to pure alumina at the same temperature in Fig. 6. This improvement is likely due to the enhanced interaction between the alumina matrix and the eggshell particles, which strengthens the material structure and also formation of a solid secondary phase, Grossite ($CaAl_4O_7$) is a calcium aluminate phase that forms during the reaction between calcium (from the eggshell) and alumina (Al_2O_3). This phase exhibits considerable thermal stability along with strength. The presence of this secondary phase can improve the mechanical integrity due to improved bonding at grain boundaries, which is more resistant to crack propagation. The proof of grossite was shown in Fig. 3C using XRD [26, 27].

The critical result of this work is that the presence of eggshells significantly reduces the shrinkage in all samples. As reported in Table 4, this effect does not change with changing sintering temperature. The side effect of the pore former can be seen in Table 5. Shrinkages are found to have been moderated effectively in all the samples with the addition of eggshells. For instance, in samples 90-2, the linear and diametral shrinkage is 6.21% and 6.32%, respectively, half the shrinkage of the pure alumina support shown in Table 4. As the pore former particle size increases, the shrinkage decreases. In sample 60-2,

Table 5. Shrinkage and porosity of ceramic membrane with the addition of Egg Shell

Membrane	Linear Shrinkage (%) ±SD	Diametral Shrinkage (%) ±SD	Porosity (%) ±SD
30-0	0.01 ± 0.01	0.12 ± 0.02	54.23 ± 1.0
30-1	0.99 ± 0.05	1.08 ± 0.06	55.11 ± 1.0
30-2	2.79 ± 0.08	2.61 ± 0.10	57.23 ± 1.2
60-0	0.12 ± 0.01	0.25 ± 0.02	50.34 ± 1.1
60-1	1.25 ± 0.04	1.52 ± 0.05	53.89 ± 1.1
60-2	4.79 ± 0.10	4.33 ± 0.12	55.02 ± 1.3
90-0	2.35 ± 0.07	2.53 ± 0.08	49.13 ± 1.2
90-1	4.78 ± 0.10	5.02 ± 0.11	51.63 ± 1.3
90-2	6.21 ± 0.12	6.32 ± 0.13	54.24 ± 1.4

Table 6. Comparison with other works reported in the literature

Reference	Composition	Forming Method	Sintering(°C)	Porosity (%)	Strength (MPa)	flux (LMH)
[30]	Natural clay + 2.5% Egg shell + 2.5% Manioc Starch	Extrusion, uniaxial compression	1100	30.66-59.05	8.75-16.9	-
[14]	Clay + Coconut husks + Eggshells	Hydraulic Pressing	900	52	2.04	14013
[31]	$Al_2Si_2O_5$ + $CaCO_3$	Phase Inversion	1250	55	-	350
[32]	Kaolin + $CaMg(CO_3)_2$ + Methocel + Amijel	Dry Pressing, Hand Roll Pressing, Extrusion	1250	43	27.72	-
[33]	Caly + CaO	Casting	800, 900, 1000	15	4.8	-
[34]	Alumina+ $CaCO_3$	Uniaxial compaction	1300, 1350, 1375, 1400	37.5	25	-
[35]	kaolin+ $CaCO_3$	Pressing, Extrusion	1300	55	28	400-1100
[36]	Kaolin+Bentonite+Limestone	uniaxial pressing	1150	44	4.48	179-755
[37]	$Al_2Si_2O_5(OH)4$+$CaCo_3$+ TiO_2 layer	Extrusion	1200	52.3	78	760
This work	Alumina+ Eggshell	Gel casting	1250-1350-1450	57.23	4.94	1860

the linear and diametral shrinkage are 4.79% and 4.33%, while in sample 30-2, the linear and diametral shrinkage are 2.79% and 2.61%. The pore former affects shrinkage. Increasing the size of pore former particles results in larger pores that, by preventing densification, impede the sintering process and, therefore, decrease shrinkage with increased size of the pore former particles. The higher the particle size of the pore former, the lower both linear and diametral material shrinkage would be because its potential for densification would be reduced. As demonstrated in Table 5, the porosity of ceramic membranes is significantly influenced by the pore-forming particles' size and the sintering temperature. The data shows that as the particle size of the pore former decreases, the porosity correspondingly reduces. Larger eggshell particles, such as those used in the 30 series, introduce larger voids into the ceramic matrix, resulting in higher porosity.

While larger pore-former particles create larger voids, resulting in higher porosity, smaller pore-former particles-for example, the 2 μm particles in the 90 series-create smaller voids and a denser membrane structure with lower porosity. Besides the size of the pore former, the sintering temperature also plays a crucial role in defining the final porosity of the membranes [28]. The rise in sintering temperature tends to increase porosity across all series, contrary to typical densification behavior usually observed in pure ceramics. The trend of porosity in the 30 series is such that it increases from 54.23% in the lower temperature to 57.23% in the higher temperature.

Similarly, in the case of the 90 series, the porosity increases from 49.13% to as high as 54.24% as the sintering temperature increases. The eggshell particles impede the densification with increased temperature; thus, this increase in porosity. In such a phenomenon, there is an obstruction to the packing of the ceramic particles due to the presence of these particles at an increased sintering temperature. The results represent, compared with those of Table 4, referring to pure α-Al_2O_3 membranes, a completely opposite trend. It is possible to observe, from Table 4, a decrease in porosity with the increase in temperature up to 1350-1450 °C due to typical densification, favored by high temperatures, which enhances particle rearrangement and packing at the expense of void spaces.

However, regarding the addition of eggshell as a pore former, an abnormal sintering process was induced, in which porosity increased with increasing sintering temperature, as observed in Table 5. The structure may be explained by the fact that the eggshell particles obstructed the complete densification for structural barriers inside the ceramic matrix, which, at higher temperatures, retain or increase the porosity. Pure ceramic membranes show the typical sintering behavior, with a decrease in porosity at higher temperatures. The addition of eggshell pore formers brings us the awareness of the modified response in terms of enhanced porosity with increasing temperature, due to the inhibited densification [29].

Fig. 7 shows the effect of sintering temperature and particle size of the pore-former on the flux of ceramic supports. Two keen observations are recorded from the results: with the rise in the size of pore former particles, the flux increases. For the 30 series pore former, with an average particle size of 10 μm, the flux values are 1760.18 LMH at 1250 °C, 1840.26 LMH at 1350 °C, and 1860.12 LMH at 1450 °C. For the 60 series, with an average particle size of 4 μm, the flux values are slightly lower: 1720.16 LMH at 1250 °C, 1786.25 LMH at 1350 °C, and 1810.11 LMH at 1450 °C. With the 90 series, which had an average particle size of 2 μm, flux decreases further to 1510.84 LMH at 1250 °C, 1570.25 LMH at 1350 °C, and 1620.00 LMH at 1450 °C. This may be explained by the fact that larger pores are formed within the ceramic support, allowing more increases in fluid flow through the material. Another critical trend observed is that involving the comparison of the sintering temperatures. Fig. 7 shows that in pure α-Al_2O_3 ceramic membranes, raising the sintering temperature from 1350 °C to 1450 °C typically produces a significant reduction of flux. For pure alumina, the flux decreases from 1550.00 LMH at 1350 °C to 1250.00 LMH at 1450 °C. This was due to the increased densification upon sintering with decreased pore size and, hence, overall flux. However, adding the eggshell powder to the ceramic mixture changed this observation. Indeed, adding 5% eggshell powder led to an increase in flux with the increase in sintering temperature throughout all the ranges tested. In the presence of eggshell powder, ceramic supports cease to exhibit this norm of lowered flux at higher sintering temperatures but instead exhibit increased flux even at increased sintering temperatures.

As shown in Table 6, our work exhibits one of the highest open porosities among the surveyed works (≈57.23%). It is slightly higher than kaolin–$CaCO_3$ supports (55% in [36]) and kaolinite with a TiO_2 layer (52.3% in [38]), and only marginally below the maximum reported for natural-clay/eggshell/manioc starch (59.05% in [30]). The pure-water flux (1860 LMH) outperforms the majority of supports that consist of ceramic powder and Eggsell (CaO, $CaCO_3$). Only one outlier, the low-temperature (900 °C) clay + coconut husk + eggshell support [31], shows a higher value (14013 LMH), but at the cost of very low strength (2.04 MPa).

4. CONCLUSION

The addition of eggshell powder into α-Al_2O_3 ceramic membranes, therefore, shows tremendous potential for improvement in mechanical properties and flux performance. Our work has indicated that the particle size of eggshell powder and sintering temperature are probably the two most influential factors on the final properties of the membrane. Membranes with small eggshell particles (2 μm) had better mechanical

10.22090/jwent.2026.01.02

strength and minor shrinkage owing to the formation of Grossite as a second phase that strengthens the ceramic matrix. While larger eggshell particles result in higher porosity and fluxes, they are potentially more applicable to filtration applications. These results have evidenced that using biowaste, such as eggshell powder, presents excellent opportunities for improving ceramic membrane properties and contributes to sustainable waste management. Future research could be directed toward optimizing porosity and mechanical strength to meet the requirements of specific industrial applications.

Conflict of Interest
The authors declare no conflict of interest.

Funding
This study was not supported by any funding.

Author's Contributions
Study Conception or Design: MS
Data Acquisition: MS; HT
Data Analysis or Interpretation: MS; HT
Manuscript Drafting: MS
Critical Manuscript Revision: MS; HT
All authors have approved the final manuscript and are responsible for all aspects of the work.

AI Statement
The authors confirm that no AI tools or services were used during the preparation of this work.

REFERENCES

[1] S. Mestre, A. Gozalbo, M. M. Lorente-Ayza, and E. Sánchez, "Low-cost ceramic membranes: A research opportunity for industrial application," *J Eur Ceram Soc*, vol. 39, no. 12, pp. 3392–3407, Sep. 2019, doi: 10.1016/j.jeurceramsoc.2019.03.054.

[2] N. Malik, V. K. Bulasara, and S. Basu, "Preparation of novel porous ceramic microfiltration membranes from fly ash, kaolin and dolomite mixtures," *Ceram Int*, vol. 46, no. 5, pp. 6889–6898, Apr. 2020, doi: 10.1016/j.ceramint.2019.11.184.

[3] F. Wu *et al.*, "Enhancing mechanical strength and porosity of alumina extrudates through composite processing," *Powder Technol*, vol. 446, Oct. 2024, doi: 10.1016/j.powtec.2024.120163.

[4] S. Chakraborty, R. Uppaluri, and C. Das, "Effect of pore former (saw dust) characteristics on the properties of sub-micron range low-cost ceramic membranes," *International Journal of Ceramic Engineering and Science*, vol. 2, no. 5, pp. 243–253, Sep. 2020, doi: 10.1002/ces2.10061.

[5] C. Torres-Sanchez, F. R. A. Al Mushref, M. Norrito, K. Yendall, Y. Liu, and P. P. Conway, "The effect of pore size and porosity on mechanical properties and biological response of porous titanium scaffolds," *Materials Science and Engineering C*, vol. 77, pp. 219–228, Aug. 2017, doi: 10.1016/j.msec.2017.03.249.

[6] L. C. C. K. D. O'Rourke, "Industrial ecology: a critical review".

[7] S. T. Ali, A. S. EL-Dieb, S. H. Aboubakr, and M. M. Reda Taha, "Utilization of ceramic waste powder in self-compacting concrete," in *Sustainable Construction Materials and Technologies*, International Committee of the SCMT conferences, 2016. doi: 10.18552/2016/scmt4s116.

[8] Y. Taha, M. Benzaazoua, R. Hakkou, and M. Mansori, "Natural clay substitution by calamine processing wastes to manufacture fired bricks," *J Clean Prod*, vol. 135, pp. 847–858, Nov. 2016, doi: 10.1016/j.jclepro.2016.06.200.

[9] B. Ngayakamo and A. P. Onwualu, "Recent advances in green processing technologies for valorisation of eggshell waste for sustainable construction materials," Jun. 01, 2022, *Elsevier Ltd*. doi: 10.1016/j.heliyon.2022.e09649.

[10] I. N. Najar *et al.*, "From waste management to circular economy: Leveraging thermophiles for sustainable growth and global resource optimization," Jun. 01, 2024, *Academic Press*. doi: 10.1016/j.jenvman.2024.121136.

[11] S. B. Hassan and V. S. Aigbodion, "Effects of eggshell on the microstructures and properties of Al–Cu–Mg/eggshell particulate composites," *Journal of King Saud University - Engineering Sciences*, vol. 27, no. 1, pp. 49–56, Jan. 2015, doi: 10.1016/j.jksues.2013.03.001.

[12] I. S. Vilarinho, E. Filippi, and M. P. Seabra, "Development of eco-ceramic wall tiles with bio-CaCO3 from eggshells waste," *Open Ceramics*, vol. 9, Mar. 2022, doi: 10.1016/j.oceram.2022.100220.

[13] V. O. Bilici, G. Pesmen, A. Yonetken, and A. Erol, "Effect of variation of egg-shell particulate reinforcement on ultrasonic pulse velocity, attenuation, and hardness prediction in ceramic-metal composites," *Thermal Science*, vol. 27, no. 4, pp. 3179–3188, 2023, doi: 10.2298/TSCI2304179B.

[14] P. Kamgang-Syapnjeu *et al.*, "Elaboration of a new ceramic membrane support from Cameroonian clays, coconut husks and eggshells: Application for Escherichia coli bacteria retention," *Appl Clay Sci*, vol. 198, Nov. 2020, doi: 10.1016/j.clay.2020.105836.

[15] "Standard Test Method for Water Absorption, Bulk Density, Apparent Porosity, and Apparent Specific Gravity of Fired Whiteware Products 1." [Online]. Available: www.astm.org

[16] A. International and files indexed by mero, "Static Tests of Lumber in Structural Sizes 1."

[17] J. Fruhstorfer and C. G. Aneziris, "Influence of particle size distributions on the density and density gradients in uniaxial compacts," *Ceram Int*, vol. 43, no. 16, pp. 13175–13184, Nov. 2017, doi: 10.1016/j.ceramint.2017.07.011.

[18] N. Shimoi and S. Kumon, "Synthesis of high-purity and high-crystallinity single-walled carbon nanotubes homogeneously dispersed by wet process," *Advanced Powder Technology*, vol. 33, no. 11, Nov. 2022, doi: 10.1016/j.apt.2022.103825.

[19] S. Balu, M. V. Sundaradoss, S. Andra, and J. Jeevanandam, "Facile biogenic fabrication of hydroxyapatite nanorods using cuttlefish bone and their bactericidal and biocompatibility study," *Beilstein Journal of Nanotechnology*, vol. 11, pp. 285–295, 2020, doi: 10.3762/bjnano.11.21.

[20] S. K. Manchili, J. Wendel, M. Vattur Sundaram, E. Hryha, and L. Nyborg, "Comparative study on the densification of chromium pre-alloyed powder metallurgy steel through nanopowder addition using design of experiments," *Results in Materials*, vol. 10, Jun. 2021, doi: 10.1016/j.rinma.2021.100173.

[21] D. D. Athayde, L. F. S. Lima, P. G. Weidler, A. M. Almeida Silva, and W. L. Vasconcelos, "Microstructure Evolution During the

Sintering of Freeze-Cast Alumina," *Materials Research*, vol. 27, 2024, doi: 10.1590/1980-5373-MR-2023-0380.

[22] Q. Li *et al.*, "Balancing flexural strength and porosity in DLP-3D printing Al2O3 cores for hollow turbine blades," *J Mater Sci Technol*, vol. 104, pp. 19–32, Mar. 2022, doi: 10.1016/j.jmst.2021.05.077.

[23] D. D. Athayde *et al.*, "Manufacture of Highly Porous Tubular Alumina Substrates with Anisotropic Pore Structure by Freeze-Casting," *Adv Eng Mater*, vol. 22, no. 7, Jul. 2020, doi: 10.1002/adem.201901432.

[24] S. Iaich, Y. Miyah, L. Messaoudi, and B. Abdellah Fez, "Moroccan Journal of Chemistry Elaboration and characterization of low cost tubular ceramic supports made of Moroccan clay for microfiltration and ultrafiltration membranes," 2021. [Online]. Available: http://revues.imist.ma/?journal=morjchem&page=login

[25] M. R. Mazlan *et al.*, "Necking mechanism under various sintering process parameters – A review," Mar. 01, 2023, *Elsevier Editora Ltda*. doi: 10.1016/j.jmrt.2023.01.013.

[26] U. Sabu *et al.*, "On the formation of α-alumina single crystal platelets through eggshell membrane bio-templating," *Scr Mater*, vol. 195, Apr. 2021, doi: 10.1016/j.scriptamat.2020.113716.

[27] Y. Huang, N. Hu, Y. Ye, Z. Ou, and X. Shi, "Preparation and pore-forming mechanism of MgO–Al2O3–CaO-based porous ceramics using phosphorus tailings," *Ceram Int*, vol. 48, no. 20, pp. 29882–29891, Oct. 2022, doi: 10.1016/j.ceramint.2022.06.253.

[28] Z. Baig, O. Mamat, M. Mustapha, A. Mumtaz, S. Ali, and M. Sarfraz, "Surfactant-decorated graphite nanoplatelets (GNPs) reinforced aluminum nanocomposites: sintering effects on hardness and wear," *International Journal of Minerals, Metallurgy and Materials*, vol. 25, no. 6, pp. 704–715, Jun. 2018, doi: 10.1007/s12613-018-1618-3.

[29] R. Vicente, K. Cesca, A. F. V. da Silva, D. de Oliveira, C. J. de Andrade, and A. Ambrosi, "Hierarchical membrane by centrifugal casting and effects of incorporating activated carbon as pore-former," *J Eur Ceram Soc*, vol. 43, no. 8, pp. 3447–3453, Jul. 2023, doi: 10.1016/j.jeurceramsoc.2023.02.040.

[30] L. Alves Xavier, T. V. de Oliveira, W. Klitzke, A. B. Mariano, D. Eiras, and R. B. Vieira, "Influence of thermally modified clays and inexpensive pore-generating and strength improving agents on the properties of porous ceramic membrane," *Appl Clay Sci*, vol. 168, pp. 260–268, Feb. 2019, doi: 10.1016/j.clay.2018.11.025.

[31] M. A. Abdulhameed, M. H. Rahman, and H. N. Azziz, "High Porous Ceramic for Oil/Water Separation: Calcite as a Sintering Aid," *Journal of Ecological Engineering*, vol. 24, no. 7, pp. 88–95, 2023, doi: 10.12911/22998993/163348.

[32] F. Bouzerara, A. Harabi, S. Achour, and A. Larbot, "Porous ceramic supports for membranes prepared from kaolin and doloma mixtures," *J Eur Ceram Soc*, vol. 26, no. 9, pp. 1663–1671, 2006, doi: 10.1016/j.jeurceramsoc.2005.03.244.

[33] B. Ngayakamo, A. M. Aboubakar, C. G. Komadja, A. Bello, and A. P. Onwualu, "Eco-friendly use of eggshell powder as a bio-filler and flux material to enhance technological properties of fired clay bricks," *Metallurgical and Materials Engineering*, vol. 27, no. 3, pp. 371–383, Sep. 2021, doi: 10.30544/628.

[34] C. Falamaki, M. Naimi, and A. Aghaie, "Dual behavior of CaCO3 as a porosifier and sintering aid in the manufacture of alumina membrane/catalyst supports," *J Eur Ceram Soc*, vol. 24, no. 10–11, pp. 3195–3201, Sep. 2004, doi: 10.1016/j.jeurceramsoc.2003.10.041.

[35] A. Harabi, F. Zenikheri, B. Boudaira, F. Bouzerara, A. Guechi, and L. Foughali, "A new and economic approach to fabricate resistant porous membrane supports using kaolin and CaCO3," *J Eur Ceram Soc*, vol. 34, no. 5, pp. 1329–1340, May 2014, doi: 10.1016/j.jeurceramsoc.2013.11.007.

[36] O. Mountoumnjou, A. Szymczyk, E. E. Lyonga Mbambyah, D. Njoya, and A. Elimbi, "New Low-Cost Ceramic Microfiltration Membranes for Bacteria Removal," *Membranes (Basel)*, vol. 12, no. 5, May 2022, doi: 10.3390/membranes12050490.

[37] F. Zenikheri, A. Harabi, F. Bouzerara, B. Boudaira, and A. Guechi, "Elaboration and characterization of tubular supports for membranes Microfiltration," *J Mater*, vol. 3, no. 1, 2015.